Pramana – J. Phys. (2022) 96:214
https://doi.org/10.1007/s12043-022-02444-6

Quasifission and fusion–fission lifetimes for successful and unsuccessful reactions to synthesise superheavy elements

P S DAMODARA GUPTA[1,2], H C MANJUNATHA[1,*], N SOWMYA[1,*] and T GANESH[2]

[1]Department of Physics, Government College for Women, Kolar 563 101, India
[2]Department of Physics, Rajah Serfoji Government College, Thanjavur 613 005, India (affiliated to Bharathidasan University, Tiruchirappalli 620 024, India)
*Corresponding authors. E-mail: manjunathhc@rediffmail.com; sowmyaprakash8@gmail.com

MS received 16 April 2022; accepted 11 June 2022

Abstract. We have systematically studied quasifission (QF) and fusion–fission (FF) lifetimes for heavy ion fusion reactions which were used in the synthesis of superheavy elements (SHEs) 104 to 118 as well as attempted to synthesise SHEs 119 and 120 using the DNS model. The dependence of QF on energy, angular momentum, entrance channel parameters, deformation parameters and orientation angles are studied. The study reveals that QF lifetimes are larger for the successful reactions than for the unsuccessful reactions. It is also observed that the study of FF lifetimes of both successful and unsuccessful reactions will not give any clue for the reason of failure of experiments to synthesise superheavy elements. It is also observed that the QF process can be controlled by the projectile of lightly deformed or spherical nuclei. The present study finds the importance in selecting the projectile–target combination for the synthesis of SHEs with $Z = 119$ and 120.

Keywords. Fusion–fission; quasifission; nuclear physics; compound nucleus; fusion.

PACS Nos 25.70.Jj; 25.70.Gh; 25.85.-w

1. Introduction

Superheavy elements (SHEs) are synthesised using heavy ion fusion reactions. In such reactions, quasifission (QF) and fusion–fission (FF) process are expected to strongly suppress the formation of an evaporation residue at higher excitation energies. At projectile energies above the fusion barrier, the fission barriers vanish due to angular momentum effects resulting in the fast splitting of the dinuclear systems before the formation of the compound nucleus [1]. The SHEs with Z=114–118 were synthesised using hot fusion reactions at their higher excitation [2,3]. SHE with $Z > 118$ are synthesised using the hot fusion reactions with ^{48}Ca projectiles and actinide targets which requires a deeper understanding of QF and FF components. Fusion–fission time-scale is greater than QF [4–6] and QF is characterised by the target/projectile nuclei. The process of QF in heavy-ion collisions was discovered by Heusch and collaborators [7]. It is important to study QF because it is one of the primary reaction mechanism that limits the formation of superheavy nuclei [8,9].

Nuclear deformation plays an important role in QF and FF. The collisions with the tips of the deformed target nucleus leads to QF, whereas collisions with the sides leads to FF [10,11]. The sub-barrier QF is observed during the collisions of deformed prolate actinide in heavy element formation reactions [12]. Orientation of the deformed target nuclei affects the fragment mass distributions in QF [13]. Projectiles with small isospin asymmetry reduce QF and are thus expected to increase the probability for fusion. For instance, reactions with neutron-rich ^{48}Ca on heavy targets have small isospin asymmetry, and thus are more favourable to fusion than reactions with ^{40}Ca [14]. Study of the orientation dependence of shell effects in QF is also an important aspect of the synthesis of superheavy nuclei [15]. Fusion probability decreases exponentially with increasing mean fissility due to QF and FF of the composite system [16]. Quasifission plays an important role in determining fusion probability [17].

Published online: 26 October 2022

In the collision of heavy ion, fragments arising either from QF and FF have very similar properties. Therefore, discrimination between QF and FF events is impossible. The main difference between the two processes is in the involved reaction time. Study of QF and FF time-scales are important in understanding the stability of superheavy element (SHE) [18]. Meanwhile, it has been observed that the survival of the compound nucleus will be comparably large for neutron-rich superheavy nuclei [2]. The main obstacle to form superheavy nuclei is QF and FF process having time-scales of zeptoseconds (zs) and attoseconds (as), respectively [4]. Superheavy elements with $Z = 104$–118 were synthesised using heavy ion fusion reactions such as ^{50}Ti $+^{208}$Pb $\rightarrow$ Rf(104) [19], ^{50}Ti $+^{209}$Bi $\rightarrow$ Db(105) [19], ^{54}Cr $+^{208}$Pb $\rightarrow$ Sg(106) [20], ^{54}Cr $+^{209}$Bi $\rightarrow$ Bh(107) [21], ^{58}Fe $+^{208}$Pb $\rightarrow$ Hs(108) [22], ^{58}Fe$+$ ^{209}Bi $\rightarrow$ Mt(109) [22], ^{62}Ni $+^{208}$Pb $\rightarrow$ Ds(110) [23], ^{64}Ni$+^{209}$Bi $\rightarrow$ Rg(111) [24], ^{70}Zn$+^{208}$Pb $\rightarrow$ Cn(112) [25], ^{70}Zn $+^{209}$Bi $\rightarrow$ Nh(113) [26], ^{48}Ca $+^{244}$Pu $\rightarrow$ Fl(114) [27], ^{48}Ca $+^{243}$Am $\rightarrow$ Mc(115) [28],^{48}Ca$+$ ^{248}Cm $\rightarrow$ Lv(116), ^{48}Ca $+^{249}$Bk $\rightarrow$ Ts(117) [29], ^{48}Ca$+^{249}$Cf $\rightarrow$ Og(118). Meanwhile, heavy ion fusion reaction such as ^{54}Sc$+^{249}$Cf, ^{50}Ti$+^{249}$Bk, ^{51}V$+^{248}$Cm, ^{54}Cr$+^{243}$Am, ^{55}Mn$+^{244}$Pu, ^{58}Fe$+^{237}$Np, ^{59}Co$+^{238}$U, ^{50}Ti$+^{249}$Cf, ^{51}V$+^{249}$Bk, ^{54}Cr$+^{248}$Cm, ^{55}Mn$+^{243}$Am, ^{58}Fe $+^{244}$Pu, ^{59}Co $+^{237}$Np, ^{64}Ni $+^{238}$U [19] are attempted to synthesise SHE 119 and 120. In spite of many attempts, researchers failed to synthesise SHE beyond $Z = 118$.

The production cross-section decreases to the order of picobarns or less [5,30] and as a result QF and FF processes occurs. In this context, there is a need for examining QF and FF time-scales for the successful and unsuccessful fusion reactions to synthesise SHE. Certainly, this will helps to find the reason for the failure to synthesise SHEs with $Z = 119$ and 120. With this objective, we have studied the QF and FF times for all successful heavy ion fusion reaction which were used for the synthesis of SHEs with $Z = 104$–118. QF and FF times for attempted heavy ion fusion reactions to synthesise SHEs with $Z = 119$ and 120 are also studied. Many theories such as Langevin equations, time-dependent Hartree–Fock model and quantum molecular dynamics model are available in [31]. Of these models, the DNS model has become popular because of its high predictability, simplicity and versatility [32–35]. Earlier workers [36–56] have studied different decay modes in the superheavy region and predicted the possible projectile–target combinations to synthesise the superheavy nuclei. The second section of this paper explains the theory used in the study of QF and FF lifetimes. Results are explained in the third section.

2. Theory

2.1 *QF lifetime*

The nucleus–nucleus interaction potential of dinuclear system is the sum of Coulomb (V_C), rotational (V_{rot}) and nuclear (V_N) potentials given by [35]

$$V(R, Z_1, Z_2, \beta_{2i}, l) = V_C(R, Z_1, Z_2, \beta_{2i}) + V_N(R, Z_1, Z_2, \beta_{2i}) + V_{rot}(l, \beta_{2i}). \quad (1)$$

The Coulomb potential between the two nuclei of DNS system is

$$V_C(R, Z_1, Z_2, \beta_{2i}) = \frac{Z_1 Z_2}{R}e^2 + \frac{Z_1 Z_2}{R^3}e^2 \times \left[\left(\frac{9}{20\pi}\right)^{1/2}\sum_{i=1}^{2} R_i^2 \beta_{2i} P_2(\cos\alpha_i) + \frac{3}{7\pi}\sum_{i=1}^{2} R_i^2 [\beta_{2i} P_2(\cos\alpha_i)]^2\right]. \quad (2)$$

Here $\beta_i (i = 1, 2)$ are the deformation parameters of the projectile and targets, P_1 and P_2 are the Legendre polynomial. $\alpha_i (i = 1, 2)$ is the angle between the beam axis and symmetric axis. The nuclear potential is given by

$$V_N(R, Z_1, Z_2, \beta_{2i}) = V_0\left\{\exp\left[\frac{-2(R - R_{12})\alpha}{R_{12}}\right] - 2\exp\left[\frac{-(R - R_{12})\alpha}{R_{12}}\right]\right\}, \quad (3)$$

where V_0 is the strength of the potential, R_{12} and α are given in [35]. The rotational potential of the DNS system is represented as

$$V_{rot}(R, l, \beta_{2i}) = \frac{\hbar^2 \ell(\ell + 1)}{2\Im_{DNS}(R, A, \beta_{2i})}, \quad (4)$$

where ℓ is the angular momentum and $\Im_{DNS}$ is the moment of inertia of the DNS system. The driving potential $U(Z, A, R) = V - Q$, where Q is the mass excess energy. The local temperature of the DNS system is

$$\Theta_{DNS}(Z, A) = \sqrt{\left(\frac{E_{DNS} - B_{QF}}{a}\right)}, \quad (5)$$

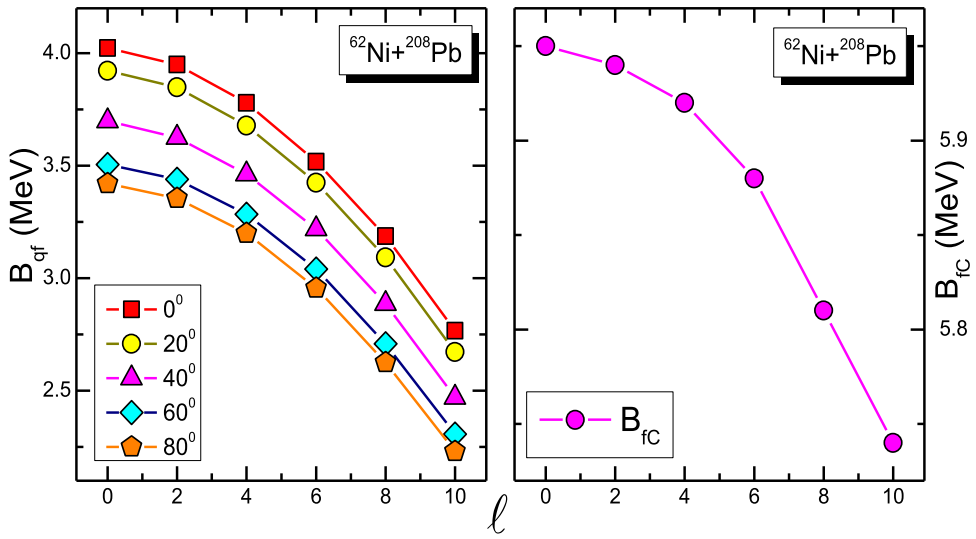

Figure 1. Angular momentum effect of fission barriers. (**a**) Variation of QF barrier with angular momentum at different orientation angles and (**b**) variation of compound nucleus fission barrier with angular momentum.

where $E_{\rm DNS} = E_{cm} - V(R_m)$ is the excitation energy of the dinuclear system and $a = 0.134A - 1.21 \times 10^{-4}A^2$ is the level density parameter. The QF decay constant $\lambda_{\rm QF}$ is defined as

$$\lambda_{\rm QF} = \frac{\omega_m}{2\pi\omega_{\rm QF}} \left(\sqrt{\left(\frac{\Gamma}{2\hbar}\right)^2 + \omega_{\rm QF}^2} - \frac{\Gamma}{2\hbar} \right) \times \exp\left(-\frac{B_{\rm QF}(Z, A, \ell)}{\Theta_{\rm DNS}(Z, A)} \right), \quad (6)$$

where $\Gamma = 2$ MeV is the average width of the contributing single-particle states near the Fermi surface and ω_m, $\omega_{\rm QF}$ are the frequency of the harmonic oscillator at $R = R_m$ and $R = R_{\rm QF}$, respectively. Inverse of the decay constant gives the QF lifetime given by

$$\tau_{\rm QF} = \frac{1}{\lambda_{\rm QF}} \quad (7)$$

2.2 *Fusion–fission lifetime*

FF decay constant is defined as

$$\lambda_{\rm FF} = \frac{1}{2\pi} \left(\sqrt{\left(\frac{\Gamma_0}{2\hbar}\right)^2 + \omega_f^2} - \frac{\Gamma_0}{2\hbar} \right) \times \exp\left(-\frac{B_f(Z, A, \ell)}{\Theta(Z, A)} \right), \quad (8)$$

where $\omega_f = 0.5$ MeV, $\Gamma_0 = 2$ MeV is the frequency of the inverted oscillator that approximate the potential in the ground state and around the top of the fission barrier and $B_f(\ell, \Theta) = cB_f^m(\ell) - h(\Theta)q(\ell)\partial W$ is the fission barrier. The nuclear temperature depending on the level density parameter a is given by

$$\Theta(Z, A) = \sqrt{\frac{E^*_{\rm CN}(l)}{a}}, \quad (9)$$

where $E^*_{\rm CN}(l) = E_{\rm CM} + Q - V^{\rm CN}_{\rm rot}$ is the excitation energy of the compound nucleus. The FF lifetime is obtained as

$$\tau_{\rm FF} = \frac{1}{\lambda_{\rm FF}}. \quad (10)$$

3. Result and discussion

To investigate the reason for the failure of the attempted fusion reactions to synthesise new elements, we have studied the QF and FF lifetimes for the heavy ion fusion reaction which were used for the synthesis of SHEs with $Z = 104$–118. We also studied the QF and FF times for attempted heavy ion fusion reactions to synthesise SHEs with $Z = 119$ and 120.

QF barriers are important parameters in the calculation of QF lifetimes. Superheavy elements are synthesised using cold/hot fusion reactions at certain excitation energies. As the excitation energies increase, the angular momentum of the compound nucleus increases. We have studied the variation of QF barriers ($B_{\rm QF}$) as a function of angular momentum (ℓ). For instance, we have plotted $B_{\rm QF}$ as a function of ℓ for the system ^{62}Ni $+^{208}$Pb which was used in the synthesis of the superheavy element darmstadtium (Ds) and is shown in figure 1.

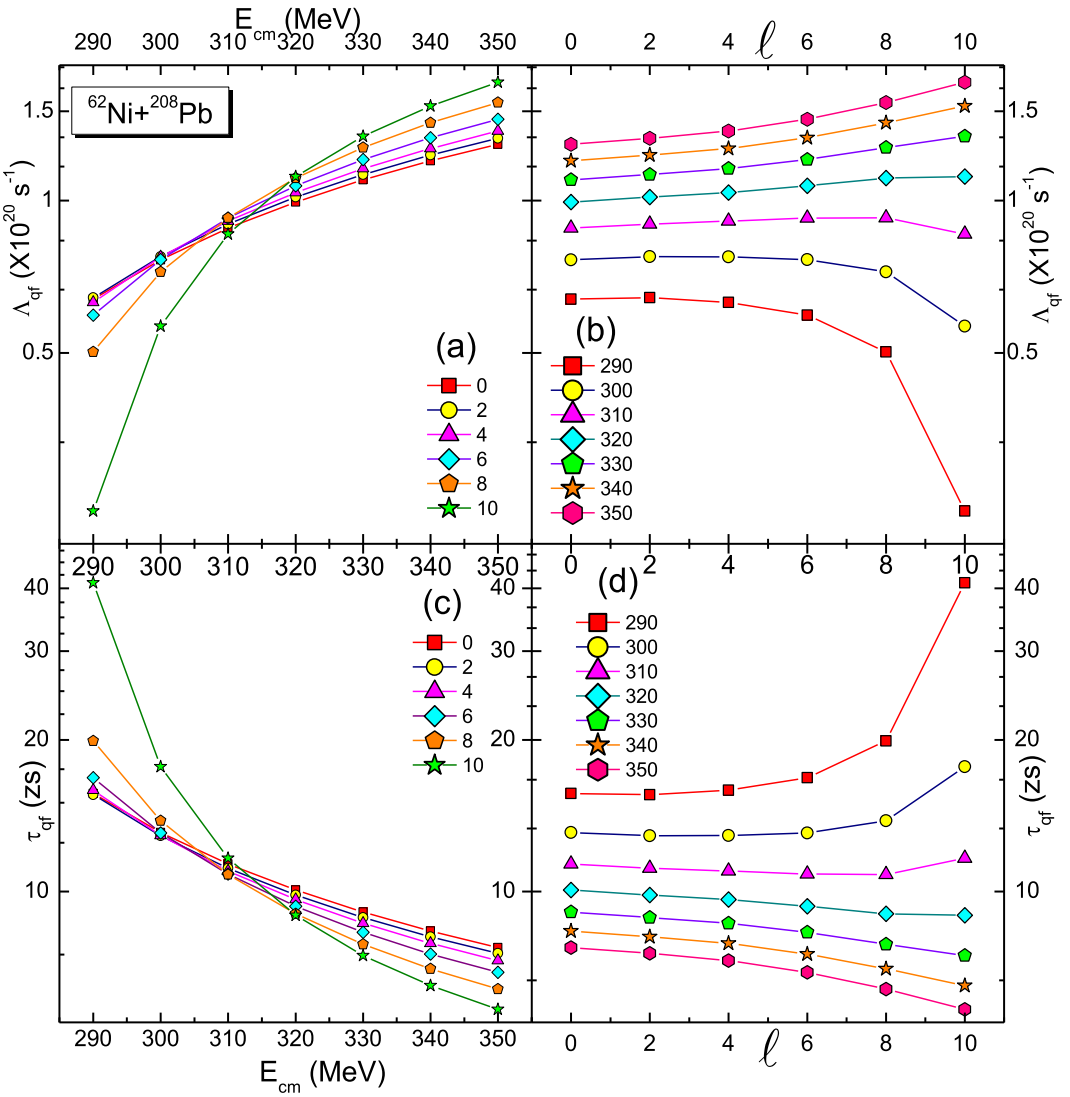

Figure 2. Dependence of QF on angular momentum (ℓ) and centre of mass energy (E_{CM}). (**a**) Variation of QF decay constant with E_{CM} at different ℓ, (**b**) variation of QF decay constant with ℓ at different E_{CM}, (**c**) variation of QF lifetime with E_{CM} at different ℓ and (**d**) variation of QF lifetime with ℓ at different E_{CM}.

First layer of figure1a shows the variation of QF barrier with angular momentum at different orientation angles. From this variation, it is found that B_{QF} decreases with increase in ℓ at different orientations of the target. Furthermore, fission barriers of the compound nucleus plays an important role in the FF process. Figure 1b shows the variation of the compound nucleus fission barrier (B_{fc}) with ℓ. This figure also shows that B_{fc} decreases with increase in ℓ. Similar variation is observed for all the successful and unsuccessful fusion reactions to synthesise SHE.

Quasifission process depends on the centre-of-mass energy (E_{CM}) and hence the angular momentum (ℓ) of the compound nucleus. Dependence of QF on angular momentum (ℓ) and centre of mass energy (E_{CM}) for the system ^{62}Ni $+^{208}$ Pb which was used in the synthesis of the superheavy element darmstadtium (Ds) is depicted in figure 2. First layer of this figure 2a shows the variation of quasifission decay constant (Λ_{QF}) with E_{CM} for different ℓ values. From this variation, it is observed that Λ_{QF} increases with increase in E_{CM}. As a result, QF lifetime (τ_{QF}) decreases with increase in E_{CM} for different ℓ values and is shown in figure 2c. From figures 2b and 2d, it is surprisingly found that τ_{QF} slightly increases with increase in the angular momentum up to $E_{\mathrm{CM}} = 310$ MeV, and afterwards, τ_{QF} decreases with increase in the angular momentum.

Fusion–fission process also depends on the angular momentum of the compound nuclei (ℓ) and E_{CM}. For instance, the dependence of FF on ℓ and E_{CM} for the system ^{62}Ni $+^{208}$Pb is also shown in figure 3. The variation of FF decay constant (Λ_{FF}) with E_{CM} at different ℓ is shown in figure 3a. Variation of Λ_{FF} with ℓ at different E_{CM} is shown in figure 3b. Figure 3c depicts that

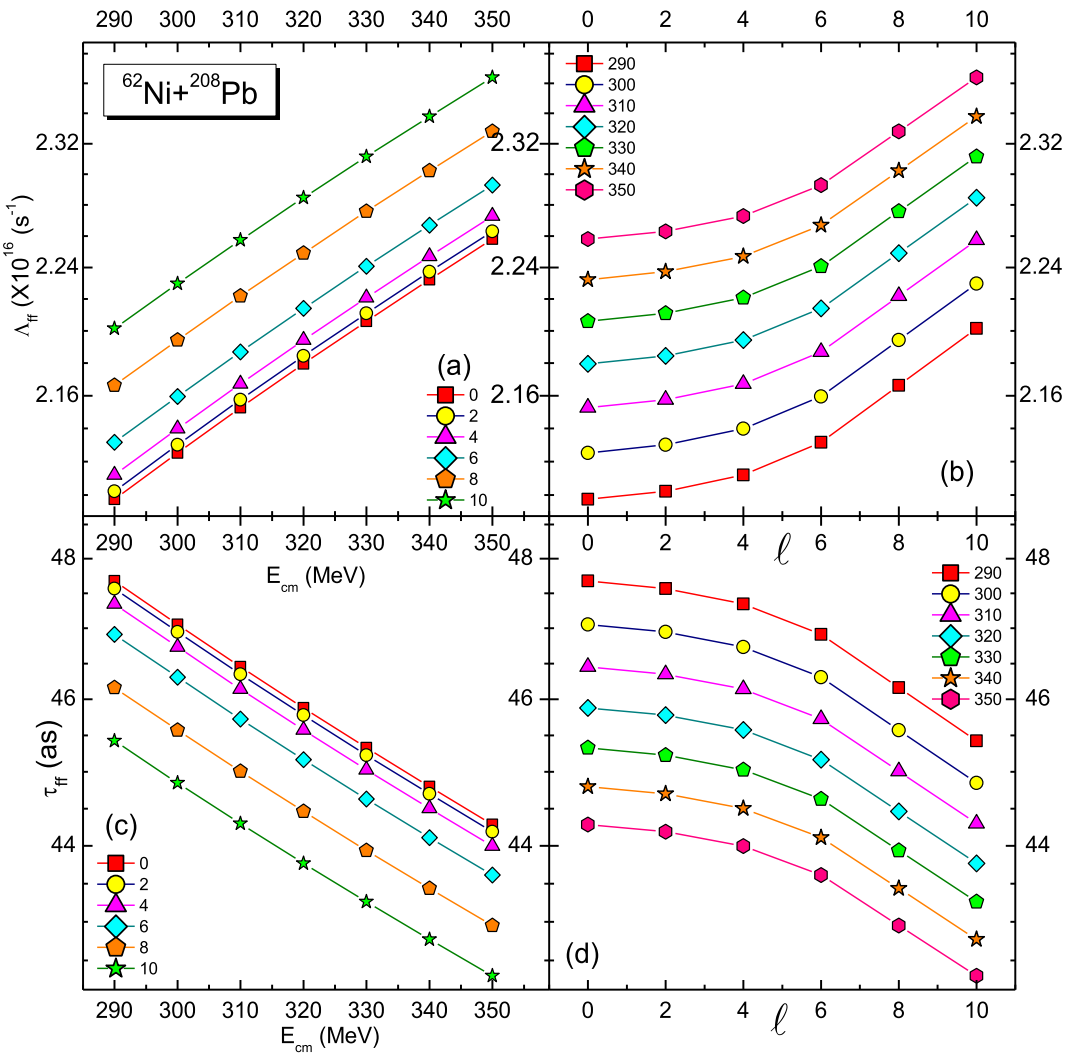

Figure 3. Dependence of FF on angular momentum (ℓ) and centre of mass energy (E_{CM}). (**a**) Variation of FF decay constant with E_{CM} at different ℓ, (**b**) variation of FF decay constant with ℓ at different E_{CM}, (**c**) variation of FF lifetime with E_{CM} at different ℓ and (**d**) variation of FF lifetime with ℓ at different E_{CM}.

FF half-lives (τ_{FF}) decrease with increase in E_{CM}. Figure 3d shows that τ_{FF} decreases with increase in ℓ at different E_{CM}.

Quasifission process is also orientation-dependent. As an illustration, we have plotted QF decay constant and half-life as a function of orientation angle for the system ^{62}Ni+^{208}Pb in figure 4. From this figure, it is evident that QF half-lives decrease with increase in the orientation angle.

The entrance channel plays a major role in the dynamic evolution of a dinuclear system. We have studied the variation of τ_{QF} and τ_{FF} with entrance channel parameters such as product of projectile and target charges (Z_1Z_2), Coulomb interaction parameters $z = Z_1Z_2/(A_1^{1/3} + A_2^{1/3})$, charge asymmetry $\alpha_z = |(Z_1 - Z_2)/(Z_1 + Z_2)|$, mass asymmetry $\eta = |(A_1 - A_2)/(A_1 + A_2)|$ and isospin asymmetry $\Delta(N/Z) = \left|(N/Z)_P - (N/Z)_T\right|$ are studied. τ_{QF} increases with increase in Z_1Z_2 and z and it is shown in figures 5a and 5b, whereas τ_{QF} decreases with increase in z, α_z and $\Delta(N/Z)$ | and it is shown in figures 5c and 5e. Fusion–fission times (τ_{FF}) decreases with increase in Z_1Z_2, z and $\Delta(N/Z)$ | and is depicted in figures 5f–5j. Fusion–fission times (τ_{FF}) increases with increase in z and α_z and it is also shown in figures 5h and 5i.

The details of cold (104–113) and hot (114–118) fusion reactions used in the synthesis of SHEs are presented in table 1. Fusion barriers (B_{fu}) of the corresponding fusion reactions are given in the second column. Energies at which the SHEs 104–118 were synthesised are given in the third (excitation energy E^*) and fourth (centre of mass energy E_{CM}) column

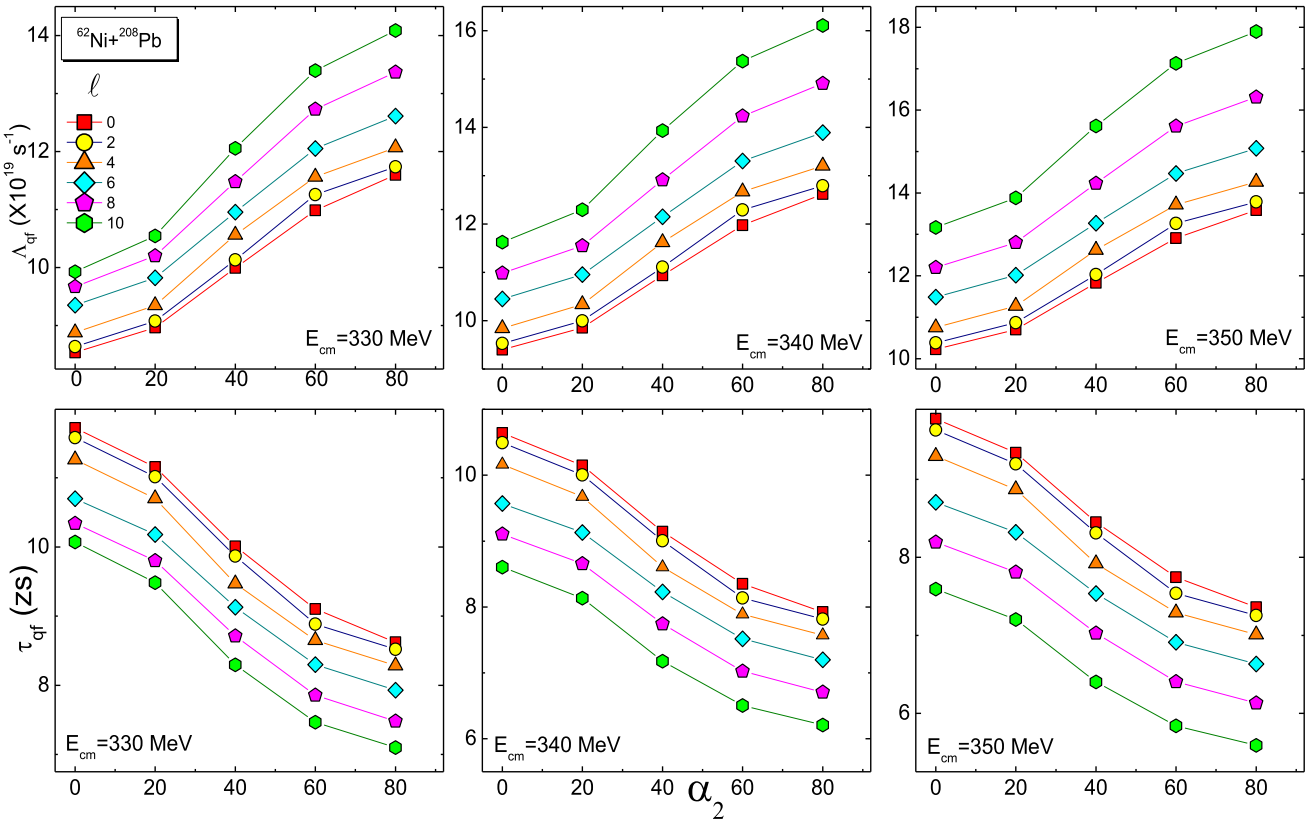

Figure 4. Variation of QF decay constant with orientation angle for different angular momenta at the centre of mass energies 330 MeV (**a**), 340 MeV (**b**) and 350 MeV (**c**). Variation of QF lifetimes with orientation angle for different angular momenta at the centre of mass energies 330 MeV (**d**), 340 MeV (**e**) and 350 MeV (**f**).

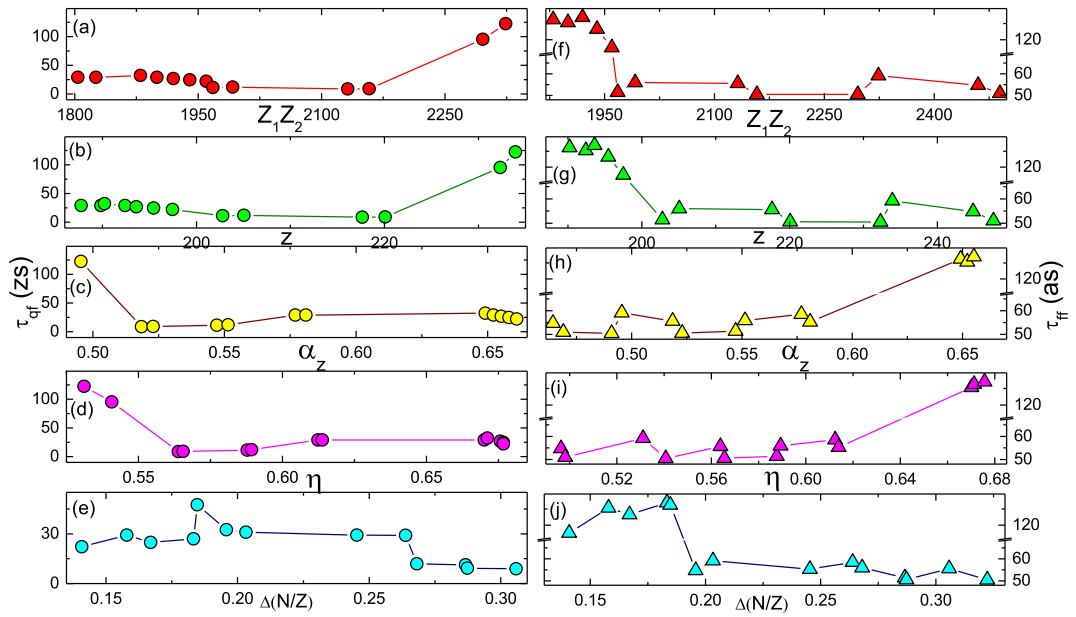

Figure 5. Variation of τ_{QF} and τ_{FF} as a function of entrance channel parameters for both hot and cold fusion reactions used in the synthesis of SHEs (104–118).

Table 1. Cold fusion and hot fusion reactions, fusion barriers (B_{fu}) [57], experiment excitation energy (E^*) and centre of mass energy (E_{CM}), average angular momentum ($\langle\ell\rangle$) [58], QF barrier (B_{QF}), QF time (τ_{QF}), compound nucleus fission barrier (B_{fC}), FF time (τ_{FF}), quadrupole deformation of projectile (β_{2p}), target (β_{2t}) and compound (β_{2c}) [59], entrance channel parameter [60] product of charges (Z_1Z_2), Coulomb interaction parameters (z), mass asymmetry (η), charge asymmetry (α_Z), isospin asymmetry ($\Delta(N/Z)$), experiment evaporation cross-section (σ_{ER}).

Reaction	B_{fu} (MeV)	E^* (MeV)	E_{CM} (MeV)	$\langle\ell\rangle$	B_{QF} (MeV)	τ_{QF} (zs)	B_{fC} (MeV)	τ_{FF} (as)	β_2			Entrance channel parameters					σ_{ER}
									Proj.	Targ.	Comp.	Z_1Z_2	z	η	α_z	$\Delta\left(\frac{N}{Z}\right)$	
$^{50}_{22}Ti + ^{208}_{82}Pb \rightarrow ^{256}_{104}Rf + 2n$ [19]	191.89	21.5	188.4	45.26	5.20	35697.28	6.26	66.70	0	0	0.247	1804	187.74	0.61	0.58	0.26	12.2^{+1}_{-1}nb
$^{50}_{22}Ti + ^{209}_{83}Bi \rightarrow ^{256}_{105}Db + 3n$ [19]	194.31	30	201.7	31.69	5.10	632.03	6.05	60.86	0	0	0.247	1826	189.84	0.61	0.58	0.25	190^{+40}_{-40}pb
$^{54}_{24}Cr + ^{208}_{82}Pb \rightarrow ^{260}_{106}Sg + 2n$ [20]	207.90	23.5	208.8	41.69	2.57	62.10	5.84	55.39	0.18	0	0.239	1968	202.79	0.59	0.55	0.29	$0.28^{+0.05}_{-0.05}$nb
$^{54}_{24}Cr + ^{209}_{83}Bi \rightarrow ^{262}_{107}Bh + 1n$ [21]	210.02	19.6	209.3	42.53	2.47	61.03	6.2	60.36	0.18	0	0.239	1992	205.06	0.59	0.55	0.27	163^{+34}_{-34}pb
$^{58}_{26}Fe + ^{208}_{82}Pb \rightarrow ^{265}_{108}Hs + 1n$ [22]	220.88	13.3	221.9	61.57	1.63	23.76	6.26	58.43	0.199	0	0.23	2132	217.64	0.56	0.52	0.31	60^{+14}_{-14}pb
$^{58}_{26}Fe + ^{209}_{83}Bi \rightarrow ^{266}_{109}Mt + 1n$ [22]	222.96	13.4	225.6	46.91	1.52	20.68	5.88	52.57	0.199	0	0.23	2158	220.08	0.57	0.52	0.29	$7.4^{+4.8}_{-3.3}$pb
$^{62}_{28}Ni + ^{208}_{82}Pb \rightarrow ^{269}_{110}Ds + 1n$ [23]	234.85	15.6	239.6	67.20	4.02	975.61	5.95	51.28	−0.096	0	0.221	2296	232.32	0.54	0.49	0.32	$3.3^{+6.2}_{-2.7}$pb
$^{64}_{28}Ni + ^{209}_{83}Bi \rightarrow ^{272}_{111}Rg + 1n$ [24]	236.73	12.5	245.6	72.35	4.05	380.33	6.62	59.60	−0.087	0	0.221	2324	233.93	0.53	0.50	0.23	$3.5^{+4.6}_{-2.3}$pb
$^{70}_{30}Zn + ^{208}_{82}Pb \rightarrow ^{277}_{112}Cn + 1n$ [25]	252.41	13.5	257.4	72.38	1.39	13.39	6.36	54.14	0.045	0	0.202	2460	244.87	0.50	0.46	0.20	$1^{+1.8}_{-0.4}$pb
$^{70}_{30}Zn + ^{209}_{83}Bi \rightarrow ^{278}_{113}Nh + 1n$ [26]	257.24	16.9	261.7	74.18	1.31	12.79	6.06	50.15	0.045	0	0.184	2490	247.62	0.50	0.47	0.18	55^{+150}_{-45}fb
$^{48}_{20}Ca + ^{244}_{94}Pu \rightarrow ^{288}_{114}Fl + 4n$ [27]	194.74	43	203.6	46.24	3.09	102.35	9.18	161.54	0	0.224	0.053	1880	190.22	0.67	0.65	0.20	$5.3^{+3.6}_{-2.1}$pb
$^{48}_{20}Ca + ^{243}_{95}Am \rightarrow ^{287}_{115}Mc + 4n$ [28]	197.20	46.1	211.2	46.04	2.85	61.25	9.2	153.56	0	0.224	−0.096	1900	192.41	0.67	0.65	0.16	$0.9^{+3.2}_{-0.8}$pb
$^{48}_{20}Ca + ^{248}_{96}Cm \rightarrow ^{292}_{116}Lv + 4n$ [61]	198.51	38.9	203.8	46.23	2.78	108.32	9.26	163.71	0	0.235	−0.07	1920	193.61	0.68	0.66	0.18	3.3pb
$^{48}_{20}Ca + ^{249}_{97}Bk \rightarrow ^{293}_{117}Ts + 4n$ [29]	200.50	39	211.6	46.15	2.61	85.65	8.96	146.07	0	0.235	−0.087	1940	195.46	0.68	0.66	0.17	$1.3^{+1.5}_{-0.6}$pb
$^{48}_{20}Ca + ^{249}_{98}Cf \rightarrow ^{294}_{118}Og + 3n$ [62]	202.62	36.6	210.6	42.79	2.41	160.25	8.48	125.96	0	0.235	−0.087	1960	197.47	0.68	0.66	0.14	$0.5^{+1.6}_{-0.3}$pb

Table 2. Details of the failed fusion reactions to synthesise SHEs 119 and 120 [Fusion barriers (B_{fu}) [57], excitation energy (E^*) and centre of mass energy (E_{CM}), average angular momentum ($\langle \ell \rangle$) [58], QF barrier (B_{QF}), QF time (τ_{QF}), compound nucleus fission barrier (B_{fC}), FF time (τ_{FF}), quadrupole deformation of the projectile (β_{2p}), target (β_{2t}) and compound (β_{2c}) [59], entrance channel parameters [60] product of charges ($Z_1 Z_2$), Coulomb interaction parameters (z), mass asymmetry (η), charge asymmetry (α_Z) and isospin asymmetry ($\Delta(N/Z)$)].

Reaction	B_{fu} (MeV)	E^* (MeV)	E_{CM} (MeV)	$\langle \ell \rangle$	B_{QF} (MeV)	τ_{QF} (zs)	B_{fC} (MeV)	τ_{FF} (as)	β_2			Entrance channel parameters				
									Proj.	Targ.	Comp.	$Z_1 Z_2$	z	η	α_z	$\Delta\left(\frac{N}{Z}\right)$
$^{58}_{26}$Fe + $^{237}_{93}$Np $\rightarrow$ ^{295}119 [63]	245.30	29.9	245.3	84.57	0.0058	9.29	8.06	90.23	0.22	0.22	−0.10	2418	239.85	0.60	0.56	0.28
$^{54}_{24}$Cr + $^{243}_{95}$Am $\rightarrow$ ^{297}119 [63]	229.79	31.5	248.9	84.54	0.2778	4.31	7.94	90.20	0.18	0.22	−0.08	2280	227.54	0.64	0.60	0.31
$^{50}_{22}$Ti + $^{249}_{97}$Bk $\rightarrow$ ^{299}119 [63]	217.76	32.4	232.9	62.37	1.2612	7.83	7.72	92.03	0	0.24	−0.02	2134	213.93	0.67	0.63	0.29
$^{51}_{23}$V + $^{248}_{96}$Cm $\rightarrow$ ^{299}119 [63]	223.75	36.8	241.4	73.99	0.8540	5.22	7.72	89.52	0	0.24	−0.02	2208	220.99	0.66	0.61	0.37
$^{55}_{25}$Mn + $^{244}_{94}$Pu $\rightarrow$ ^{299}119 [63]	236.56	37.7	256.5	89.99	0.0944	4.92	7.72	84.14	0.20	0.22	−0.02	2350	233.79	0.63	0.58	0.40
$^{45}_{21}$Sc + $^{249}_{98}$Cf $\rightarrow$ ^{294}119 [63]	213.53	41.7	227.2	59.01	1.1071	6.29	8.29	111.88	0	0.24	0.08	2058	208.97	0.69	0.65	0.40
$^{64}_{28}$Ni + $^{238}_{92}$U $\rightarrow$ ^{302}120 [63]	266.84	27.3	278.9	82.59	0.5470	5.14	6.07	51.45	−0.09	0.22	0	2576	252.62	0.58	0.53	0.30
$^{50}_{22}$Ti + $^{249}_{98}$Cf $\rightarrow$ ^{299}120 [63]	219.61	31.7	235.4	40.30	1.1028	6.61	7.48	84.87	0	0.24	−0.04	2156	216.14	0.67	0.63	0.27
$^{54}_{24}$Cr + $^{248}_{96}$Cm $\rightarrow$ ^{302}120 [63]	231.22	33	251	25.93	0.2381	5.01	6.07	56.25	0.18	0.24	0	2304	228.97	0.64	0.60	0.33
$^{58}_{26}$Fe + $^{244}_{94}$Pu $\rightarrow$ ^{302}120 [63]	247.01	33.9	265.7	43.01	0.0025	6.25	6.07	53.82	0.20	0.22	0	2444	241.51	0.62	0.57	0.36
$^{55}_{25}$Mn + $^{243}_{95}$Am $\rightarrow$ ^{298}120 [63]	239.90	34.5	259.6	78.99	0.0269	8.65	7.33	74.77	0.20	0.22	−0.08	2375	236.48	0.63	0.58	0.36
$^{51}_{23}$V + $^{249}_{97}$Bk $\rightarrow$ ^{300}120 [63]	225.62	35.9	243.8	41.27	0.7281	4.56	7.01	73.70	0	0.24	−0.01	2231	223.11	0.66	0.62	0.35

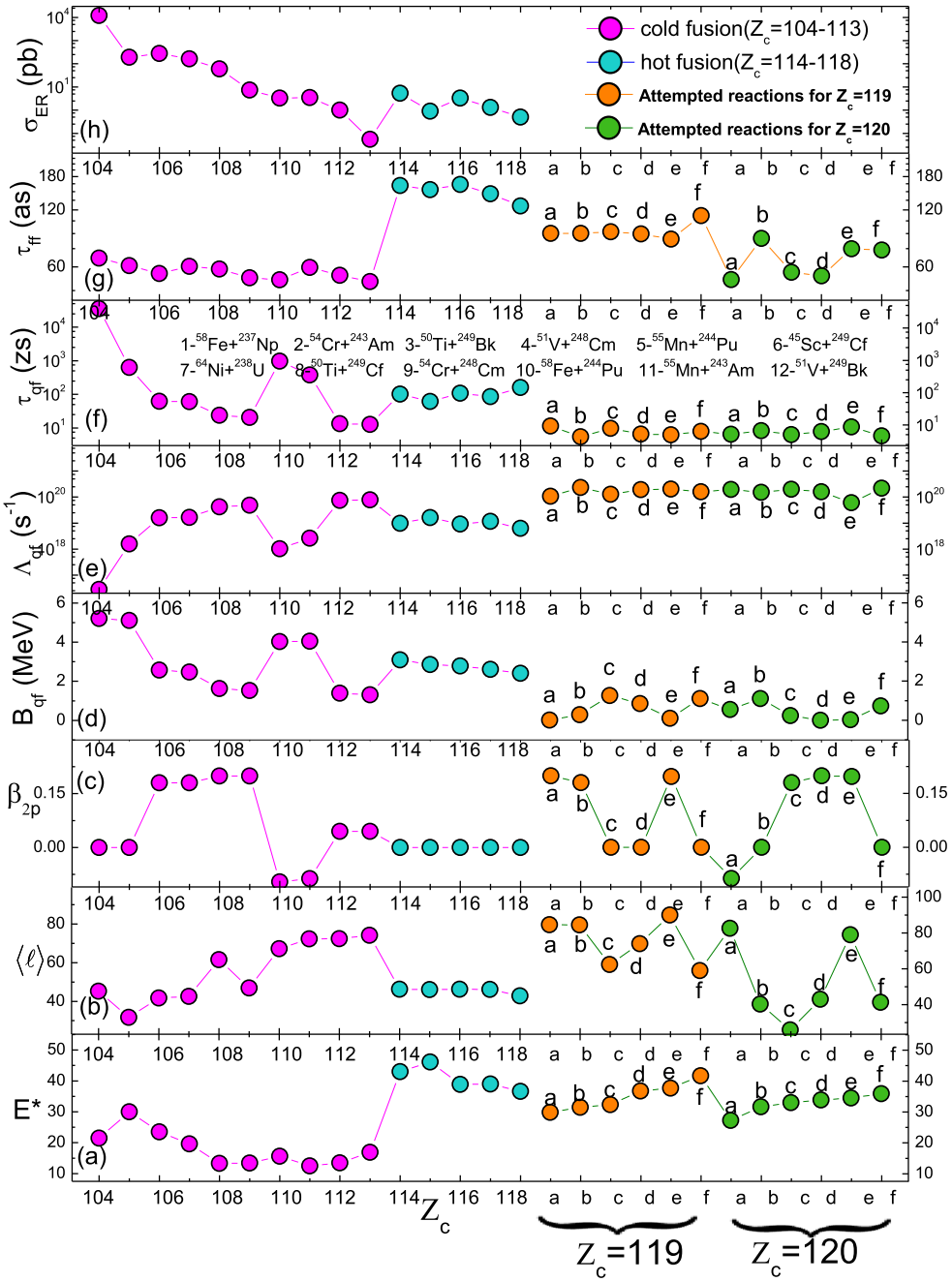

Figure 6. Excitation energy, average angular momentum, quadruple deformation parameter of the projectile, decay constant of QF, QF time scale, FF time scale and evaporation residue cross-section for the synthesised SHEs with $Z = 104 - 118$ and failed fusion reactions to synthesise SHEs with $Z = 119$ and 120.

of table 1. Angular momenta of the compound nuclei at that experimental excitation energy are shown in the fifth column. Quasifission barriers (B_{QF}) and quasifission times (τ_{QF}) evaluated using the DNS model are given in the sixth and seventh columns, respectively of this table. Eighth and ninth columns of this table present the fission barrier of the compound nucleus (B_{fc}) and FF times (τ_{FF}) of the compound nuclei formed during the synthesis of SHEs 104–118. Tenth to twelfth columns represent the quadrupole deformation parameters of the projectile, target and compound nucleus, respectively. The entrance channel parameters such as product of charges ($Z_1 Z_2$), Coulomb interaction parameters (z), mass asymmetry (η), charge asymmetry (α_Z) and isospin asymmetry ($\Delta(N/Z)$) for the cold and hot fusion reactions used in the synthesis of SHE are presented in the thirteenth to seventeenth columns of this table, respectively. Last column of table 1 presents the

production cross-section in the synthesis of SHEs (104–118). Similar details for the failed fusion reactions to synthesise superheavy elements 119 and 120 are presented in table 2.

The excitation energies at which the SHE with $Z = 104$–118 were synthesised are shown in figure 6a. In figure 6a, the excitation energies at which the experiments were attempted to synthesise the SHEs 119 and 120 are also included. It is evident from variation that SHE up to 113 were synthesised at low excitation energies (< 30 MeV) through cold fusion reactions. Superheavy elements 114–118 were synthesised at higher excitation energy (>35 MeV) through hot fusion reactions. The average angular momentum ($\langle \ell \rangle$) of the compound nuclei at excitation energies for both successful and unsuccessful reactions are shown in figure 6b. After detailed investigation, it is found that the projectile deformation parameter influences the QF process. Quadrupole deformation parameters of the projectiles used in the synthesis of SHEs 104–118 are presented in figure 6c. Figure 6c also includes quadrupole deformation parameters of the projectiles used in the failed reactions to synthesise elements 119 and 120. Quadrupole deformation parameter directly influences the QF barrier (B_{QF}). If β_2 is small, B_{QF} is large, for instance, the compound nuclei $Z = 104$, 105, 110 and 111 have smaller deformation parameters, which has comparably larger values of the QF barriers and is depicted in figure 6d. Figure 6d also shows smaller values of QF barrier for the deformed compound nuclei ($Z = 106$–109,112–118). The QF barriers of failed reactions to synthesise SHEs 119 and 120 are also included in figure 6d. This layer shows that the QF barriers for the successful reactions to synthesise the SHEs 104–118 are larger than the failed reactions to synthesise SHEs 119 and 120. Figures 6e and 6f represent the QF decay constant and QF times respectively for the synthesised SHEs 104–118 as well as for the unsuccessful fusion reactions to synthesise SHEs 119 and 120. The FF times for the compound nucleus during the synthesis of SHEs 104–118 and for the failed reactions to synthesise new SHEs 119 and 120 are shown in figure 6g. From this figure, it is found that FF times for the SHE which are synthesised using the cold fusion (104–113) reactions are smaller than that of the hot fusion reactions (114–118). Finally, evaporation residue cross-section (σ_{ER}) in the synthesis of SHEs 104–118 were presented in figure 6h. From this variation, it is observed that τ_{QF} is comparably larger for fusion reaction with oblate projectiles to synthesise the SHE ($Z = 111$ and 112). After detailed investigation, it is found that the QF lifetimes for successful fusion reactions to synthesise SHE range from 25 to 36000 zeptoseconds (zs), whereas the attempted fusion reactions to synthesise the SHE having QF lifetimes that range from 4 to 10 zs. Furthermore, FF times for successful fusion reactions to synthesise SHE ranges from 50 to165 attoseconds (as), whereas the attempted fusion reactions to synthesise the SHE are having FF lifetimes ranging from 50 to 112 as.

Quasifission process plays a major role in the synthesis of SHE. SHEs are successfully synthesised by controlling the QF process. QF process can be controlled by the deformation parameter of the projectile. Fusion reactions induced by the oblate projectile used in the synthesis of the SHE results in comparably larger QF times. This is evident in the experiments of the synthesis of SHEs 110 and 111. Fusion reactions induced by the spherical projectile (^{48}Ti) have larger QF times and it is observed in the case of SHEs 104 and 105. In cold fusion reactions with spherical projectiles, the QF times take precedence. However, in hot fusion reactions with spherical projectiles, the QF is not dominant. It can be concluded from this study that QF times are comparably larger for the fusion reactions of the spherical projectile and the target (^{50}Ti $+^{208}$Pb,^{50} Ti $+^{209}$Bi).

4. Summary

We have systematically studied QF and FF times for heavy ion fusion reactions which were used in the synthesis of SHEs 104 to 118. We have also attempted to synthesise SHEs 119 and 120 using the DNS model. The study reveals that QF lifetimes (2536000 zs) for the successful reactions which were used in the synthesis of SHE are larger than the QF times (4–10 zs) of the unsuccessful reactions for the synthesis of SHEs. It is also observed that the QF lifetimes are controlled by the deformation parameters and excitation energies.

References

[1] W U Schroder and J R Huizenga, *Treatise on heavy-ion science* **1**, 113 (1984)
[2] Y T Oganessian and V K Utyonkov, *Nucl. Phys. A* **944**, 62 (2015)
[3] J B Roberto, C W Alexander and R A Boll, *Nucl. Phys. A* **944**, 99 (2015)
[4] R du Rietz, D J Hinde, M Dasgupta, R G Thomas, L R Gasques, M Evers, N Lobanov and A Wakhle, *Phys. Rev. Lett.* **106(5)**, 052701 (2011)
[5] J Toke *et al*, *Nucl. Phys. A* **440(2)**, 327 (1985)
[6] W Q Shen *et al*, *Phys. Rev. C* **36(1)**, 115 (1987)
[7] B Heusch *et al, Z. Phys. A At. Nucl.* **288(4)**, 391 (1978)
[8] C C Sahm *et al*, *Z. Phys. A At. Nucl*. **319(2)**, 113 (1984)
[9] H Gäggeler *et al*, *Z. Phys. A At. Nucl*. **316(3)**, 291 (1984)

[10] D J Hinde *et al*, *Phys. Rev Lett.* **74(8)**, 1295 (1995)
[11] D J Hinde *et al*, *Phys. Rev. C* **53(3)**, 1290 (1996)
[12] D J Hinde *et al*, *Phys. Rev. C* **97(2)**, 024616 (2018)
[13] K Nishio *et al*, *Phys. Rev. C* **77(6)**, 064607 (2008)
[14] C Simenel *et al*, *Phys. Lett. B* **710(5)**, 607 (2012)
[15] A Wakhle *et al*, *Phys. Rev. Lett.* **113(18)**, 182502 (2014)
[16] E M Kozulin *et al*, *Phys. Rev. C* **99(1)**, 014616 (2019)
[17] K Banerjee *et al*, *Phys. Rev. Lett.* **122(23)**, 232503 (2019)
[18] M Morjean and *et al*, *Phys. Rev. Lett.* **101(7)**, 072701 (2008)
[19] F P Heßberger *et al*, *The Eur. Phys. J. A: Hadrons and Nuclei* **12(1)**, 57 (2001)
[20] G Münzenberg *et al*, *Z. Phys. A At. Nucl*. **322(2)**, 227 (1985)
[21] C M Folden III *et al*, *Phys. Rev. C* **73(1)**, 014611 (2006)
[22] S Hofmann *et al*, *Z. Phys. A: At. Nucl.* **358(4)**, 377 (1997)
[23] S Hofmann *et al*, *Z. Phys. A At. Nucl.* **350(4)**, 277 (1995)
[24] S Hofmann *et al*, *The Eur. Phys. J. A: Hadrons and Nuclei* **14(2)**, 147 (2002)
[25] S Hofmann *et al*, *Z. Phys. A At. Nucl.* **354(3)**, 229 (1196)
[26] K Morita *et al*, *J. Phys. Soc. Japan* **73(10)**, 2593 (2004)
[27] Y T Oganessian *et al*, *Phys. Rev. C* **69(5)**, 054607 (2004)
[28] Y T Oganessian *et al*, *Phys. Rev. C* **69(2)**, 021601 (2004)
[29] Y T Oganessian *et al*, *Phys. Rev. Lett.* **104(4)**, 142502 (2010)
[30] J H Hamilton, S Hofmann and Y T Oganessian, *Ann. Rev. Nucl. Part. Sci.* **63**, 383 (2013)
[31] P Wen, C Li, L Zhu, C Lin and F Zhang, *J. Phys. G: Nucl. Part. Phys.* **44(11)**, 115101 (2017)
[32] G Fazio *et al*, *J. Phys. Soc. Jpn* **77(12)**, 124201 (2008)
[33] A Nasirov *et al*, *Nucl. Phys. A* **759(3)**, 342 (2005)
[34] Khanlari, M Varasteh and S Soheyli, *Phys. Rev. C* **95(2)**, 024617 (2017)
[35] S Soheyli, M Khanlari and Varasteh, *Phys. Rev. C* **94(3)**, 034615 (2016)
[36] H C Manjunath, *Nucl. Phys. A* **945**, 42 (2016)
[37] H C Manjunath and N Sowmya, *Nucl. Phys. A* **969**, 68 (2018)
[38] H C Manjunatha, K N Sridhar and N Sowmya, *Nucl. Phys. A* **987**, 382 (2019)
[39] H C Manjunatha and K N Sridhar, *Nucl. Phys. A* **962**, 7 (2017)
[40] N Sowmya and H C Manjunatha, *Braz. J. Phys.* **49(6)**, 874 (2019)
[41] H C Manjunatha, K N Sridhar and N Sowmya, *Phys. Rev. C* **98(2)**, 024308 (2018)
[42] K N Sridhar, H C Manjunatha and H B Ramalingam, *Phys. Rev. C* **98(6)**, 064605 (2018)
[43] N Sowmya and H C Manjunatha, *Bulg. J. Phys* **46**, 16 (2019)
[44] N Sowmya and H C Manjunatha, *Braz. J. Phys.* **50(3)**, 317 (2020)
[45] N Sowmya and H C Manjunatha, *Phys. Part. Nucl. Lett.* **17(3)**, 370 (2020)
[46] H C Manjunatha, *Int. J. Mod. Phys. E* **25(9)**, 1650074 (2016)
[47] H C Manjunatha, N Sowmya, K N Sridhar and L Seenappa, *J. Radioanal. Nucl. Chem.* **314(2)**, 991 (2017)
[48] H C Manjunatha and N Sowmya, *Int. J. Mod. Phys. E* **27(5)**, 1850041 (2018)
[49] M G Srinivas, H C Manjunatha, K N Sridhar, N Sowmya and S Alfred Cecil Raj, *Nucl. Phys. A* **995**, 121689 (2020)
[50] N Sowmya, H C Manjunatha, N Dhananjaya and A M Nagaraja, *J. Radioanal. Nucl. Chem.* **323(3)**, 1347 (2020)
[51] G R Sridhar, H C Manjunatha, N Sowmya, P S Damodara Gupta and H B Ramalingam, *The Eur. Phys. J. Plus* **135(3)**, 1 (2020)
[52] H C Manjunatha and K N Sridhar, *The Eur. Phys. J. A* **53(5)**, 1 (2017)
[53] H C Manjunatha and K N Sridhar, *Nucl. Phys. A* **975**, 136 (2018)
[54] K N Sridhar, H C Manjunatha and H B Ramalingam, *Nucl. Phys. A* **983**, 195 (2019)
[55] H C Manjunatha and K N Sridhar, *Phys. Part. Nucl. Lett.* **16(6)**, 647 (2019)
[56] K N Sridhar, H C Manjunatha and H B Ramalingam, *Braz. J. Phys.* **49(2)**, 232 (2019)
[57] T Nandi, D K Swami and P S Damodara Gupta, *Private communication* (2020)
[58] O A Capurro *et al*, *Phys. Rev. C* **55(2)**, 766 (1997)
[59] P Möller, J R Nix, W D Myers and W J Swiatecki, arXiv preprint arXiv:nucl-th/9308022
[60] H C Manjunatha *et al*, *Phys. Rev. C* **102(6)**, 064605 (2020)
[61] Y T Oganessian *et al*, *Phys. Rev. C* **70(6)**, 064609 (2004)
[62] Y T Oganessian, V K Utyonkov and Y V Lobanov, *Phys. Rev. C* **74(4)**, 044602 (2006)
[63] J Khuyagbaatar, A Yakushev and C E Düllmann, GSI Helmholtzzentrum reports (2013)